Polycrystalline domain structure of pentacene thin films epitaxially grown on a hydrogen-terminated Si(111) surface

doi: 10.1103/PhysRevB.76.165424

Polycrystalline domain structure of pentacene thin films epitaxially grown on a hydrogen-terminated Si(111) surface

S. Nishikata,[1] G. Sazaki,[1,2,*] J. T. Sadowski,[1] A. Al-Mahboob,[1] T. Nishihara,[1] Y. Fujikawa,[1] S. Suto,[3] T. Sakurai,[1] and K. Nakajima[1]

[1]*Institute for Materials Research, Tohoku University, 2-1-1 Katahira, Aoba-ku, Sendai 980-8577, Japan*

[2]*Center for Interdisciplinary Research, Tohoku University, Aramaki, Aoba-ku, Sendai 980-8578, Japan*

[3]*Department of Physics, Graduate School of Science, Tohoku University, Aramaki, Aoba-ku, Sendai 980-8578, Japan*

(Received 16 November 2006; revised manuscript received 14 July 2007; published 19 October 2007)

Single-monolayer high pentacene (Pn) dendrites grown on a hydrogen-terminated Si(111) surface [H-Si(111)] under ultrahigh vacuum were observed by low-energy electron microscopy and microbeam low-energy electron diffraction analyses. We determined the epitaxial structure (type I) inside a unique polycrystalline domain structure of such dendrites, each of which has six equivalent epitaxial orientations of Pn two-dimensional (2D) unit cells. There are three sets of these cells, which are rotated ±120° relative to each other. Domain boundaries inside each dendrite were successfully observed by scanning tunneling microscopy. In addition, we found another epitaxial relation (type II): the polycrystalline domain structure and lattice parameters are similar to those of the type-I dendrite; however, the 2D unit cells of the type-II dendrite are rotated approximately 90° relative to those of the type-I dendrite. These results suggest that the crystal structure of the dendrites on H-Si(111) is determined mainly by the interaction between Pn molecules. Each dendrite is composed of domains that are exclusively of type I or II. The so-called point-on-line coincidences are found between the Pn 2D lattices of types I and II, and H-Si(111). The higher commensurability of the type-I dendrites than the type-II dendrites results in a higher probability of type-I dendrite formation. Moreover, for both the type-I and type-II dendrites, we found supercell structures. We estimated the minimum interface energy between the dendrite and H-Si(111) from an island's free energy, which is necessary to reproduce the growth of a single-monolayer high dendrite.

DOI: 10.1103/PhysRevB.76.165424 PACS number(s): 68.55.Jk, 61.66.Hq, 68.37.Nq, 61.14.Hg

I. INTRODUCTION

Recent progress in the application of organic materials in microelectronic devices has received significant attention[1–3] because of the considerable advantages these materials offer, such as flexibility, low production cost, biodegradability, and plentiful material resources. Among the currently investigated organic materials, pentacene ($C_{22}H_{14}$) appears to be particularly promising since it has been successfully used in organic thin-film transistors (OTFTs) with field-effect mobilities that match or even surpass those of amorphous silicon.[3,4] Pentacene (Pn) is a flat, elongated molecule, consisting of five π-conjugated, aromatic benzenelike rings. The bulk phase of pentacene has a triclinic crystal structure with two nonequivalent molecules per unit cell.[5–7] It has a layered structure with a herringbone arrangement of the molecules in the (001) plane. The (001) surface of a pentacene crystal has a much lower surface energy than other low-index surfaces, and the bonds between molecules in the same layer are several times stronger than those between molecules in adjacent layers. This anisotropy in bonding is the driving force for the film to exhibit a (001) "standing-up" orientation when deposited on a substrate with which it interacts weakly.[8]

To fabricate OTFTs with improved electrical properties, it is important to elucidate how the morphology of Pn thin-film crystals and their time evolution are affected by the interaction between thin films and their substrates, and by the growth kinetics under various deposition conditions. Pn thin-film crystals grow as dendrites on inert substrates.[8–10] Moreover, we have recently found that a "polycrystalline domain structure" inside a Pn dendrite develops simultaneously with the dendrite's growth on a hydrogen-terminated Si(111) surface [H-Si(111)]: hereafter, we call such a dendrite a Pn dendrite.[11] We observed the growth of single-monolayer-high Pn dendrites on H-Si(111) and found that domains with different molecular orientations inside the dendrite can be clearly depicted at different contrast levels by low-energy electron microscopy (LEEM). From *in situ* observation of the growth processes, we concluded that the key to the formation of a polycrystalline domain structure is the balance between the tendency to align the preferential growth directions of Pn two-dimensional (2D) unit cells and a supply of Pn molecules to the growth fronts of a Pn dendrite by surface diffusion. We believe that studies of the simultaneous development of the polycrystalline domain structures inside the dendrite will lead to the clarification of the importance of the precise control of the organic thin-film growth.

In this work, we present the results of a detailed study of the epitaxial structure of Pn dendrites grown on H-Si(111) and determine the correlation between the epitaxial structure and the polycrystalline domain structure inside a Pn dendrite. We analyze the commensurabilities between a Pn dendrite and H-Si(111), and discuss the origin of supercell structures. We also estimate the interface energy between a Pn dendrite and H-Si(111) by calculating the free energy of a Pn dendrite.

II. EXPERIMENT

The experiments described in this paper were carried out in an ultrahigh vacuum LEEM system (Elmitec GmbH,

LEEM III).[12] The H-Si(111) substrate was prepared according to the recipe reported by Suto *et al.*[13,14] After organic dirt on Si(111) wafers was removed by ultrasonic cleaning with trichloroethylene and acetone, the wafers were oxidized in a solution of $H_2SO_4:H_2O_2=3:1$ for 2 min and etched with NH_4F for 20 min. Before the growth of Pn thin films, the substrate was transferred to a LEEM chamber (base pressure: 5×10^{-10} Torr) and heated at 150 °C for 12 h to degas the substrate.

Pn was thermally evaporated from a tantalum crucible on the substrate kept at room temperature at deposition rates of 0.05–0.5 ML/min, where 1 ML corresponds to the molecular density of the Pn(001) plane.[5] The growth of Pn thin films was observed in real time, and in the bright-field and tilted bright-field LEEM modes,[12] at imaging electron energies not exceeding 3 eV to prevent film damage caused by electron irradiation. To observe polycrystalline domain structures inside a Pn dendrite, the tilted bright-field imaging mode was used. In this imaging mode, the contrast aperture was positioned to transmit the (00) diffraction spot, and the incident electron beam was intentionally tilted several degrees from the surface normal. The angle and direction of the beam tilt were adjusted to obtain good contrast between domains, but are not known at present. In all our experiments, the growth of Pn thin-film crystals was stopped before the H-Si(111) surface was fully covered with a Pn layer.

After the LEEM of the growth of Pn dendrites, the low-energy electron diffraction (LEED) patterns in the normal and microbeam diffraction (μ-LEED) modes were recorded at electron energies typically in the range of 10–17 eV using a fast charge coupled device camera. The first few frames of the LEED patterns obtained before the destruction of the Pn film were used for the subsequent analyses. To determine the lattice parameters of Pn dendrites, the illumination aperture of μ-LEED was set so that a selected area for the analysis included both an edge of a Pn dendrite and a bare H-Si(111) surface, and then μ-LEED patterns were observed. After H-Si(111)-related and Pn-related diffraction spots were obtained simultaneously, the instrument-induced distortion[12] of μ-LEED patterns was carefully corrected so as to obtain a regular hexagonal symmetry of the H-Si(111)-related spots.

III. RESULTS AND DISCUSSION

A. Polycrystalline domain structure

To investigate the domain structure and the epitaxial orientations of the Pn thin-film crystals grown on H-Si(111), a single-monolayer-high Pn dendrite was observed by LEEM and LEED. Figure 1(a) shows a LEEM image of a branch of the dendrite observed in the tilted bright-field mode. As reported previously,[11] the polycrystalline domain structure in the dendrite is clearly depicted at three relatively different contrast levels (hereafter called "white," "gray," and "black" for convenience of discussion). The domains with different contrast levels correspond to areas of different orientations of Pn molecules in relation to the substrate. Because the intensity of scattered electrons strongly depends on local scattering conditions, the tilted incident electron beam enabled us to visualize the domains with different molecular orientations at different contrast levels, utilizing different dependences of scattered intensity on scattering angle.

Figure 1(b) shows a selected-area LEED pattern taken from the Pn dendrite shown in Fig. 1(a). In Fig. 1(b), all domains inside the Pn dendrite as well as the bare substrate surface were observed simultaneously. Figure 1(b) shows 24 diffraction spots (indicated by arrows) from the Pn dendrite and 6 diffraction spots (marked by open circles) from the H-Si(111) surface. We also took μ-LEED patterns [Figs. 1(c) and 1(d)] from the areas indicated by the open circles c and d in Fig. 1(a) using a selected surface area of 2 μm diameter. The four diffraction spots in Figs. 1(c) and 1(d) indicate that each of areas c and d in Fig. 1(a), inside the respective domains depicted at gray and white contrast levels, is single crystalline.

Figure 1(e) shows a μ-LEED pattern taken from the area indicated by open circle e in Fig. 1(a), in which domains depicted at black and gray contrast levels are present. In Fig. 1(e), in addition to the four diffraction spots (marked by open squares) observed in area c [Fig. 1(c)], four diffraction spots (marked by open triangles), which are rotated approximately 120° from those found in areas c and d [Figs. 1(c) and 1(d)], are observed. These observations indicate that the orientations of 2D unit cells of Pn in the domains depicted at three relatively different contrast levels in Fig. 1(a) are rotated approximately 120° relative to each other.

In addition, area f in Fig. 1(a), inside the domain depicted at the gray contrast level, yields a μ-LEED pattern [Fig. 1(f)] that shows two sets of 2D unit cells with a 4.6° relative rotation. As shown in Figs. 1(c) and 1(f), some areas inside the domain depicted at one contrast level (here in gray) contribute to one set of four diffraction spots, whereas other areas yield two sets of spots with a 4.6° relative rotation. These observations clearly indicate that the domain depicted at one contrast level can also be a mixture of two orientations rotated by 4.6° with respect to each other. Although domains with approximately 120° relative rotations can be clearly visualized at different contrast levels, areas with 4.6° relative rotations cannot be distinguished in the tilted bright-field LEEM mode, owing to limitations in contrast resolution.

From these above results, we can conclude that Pn polycrystalline thin films grown on H-Si(111) have six equivalent epitaxial orientations. This number of epitaxial orientations coincides with that provided by the twofold symmetry of the Pn(001) unit cell and the threefold symmetry of H-Si(111).

Also note that we observed no difference between the LEED patterns of H-Si(111) surfaces (in neither the intensity nor distribution of the spots) taken from the clean H-Si(111) surface before the Pn deposition and those taken from the bare (not covered by the Pn dendrite) substrate surfaces after the deposition of submonolayer Pn (data are not shown). In addition, after the Pn deposition, we clearly observed monoatomic steps of the inner and outer H-Si(111) areas covered by the Pn thin-film crystals.[15] These observations prove that the crystallization of the Pn dendrite started without the formation of a wetting layer, unlike in the cases of Si(111)-7 $\times$7 and Si(001)-2$\times$1, where Pn molecules were first ran-

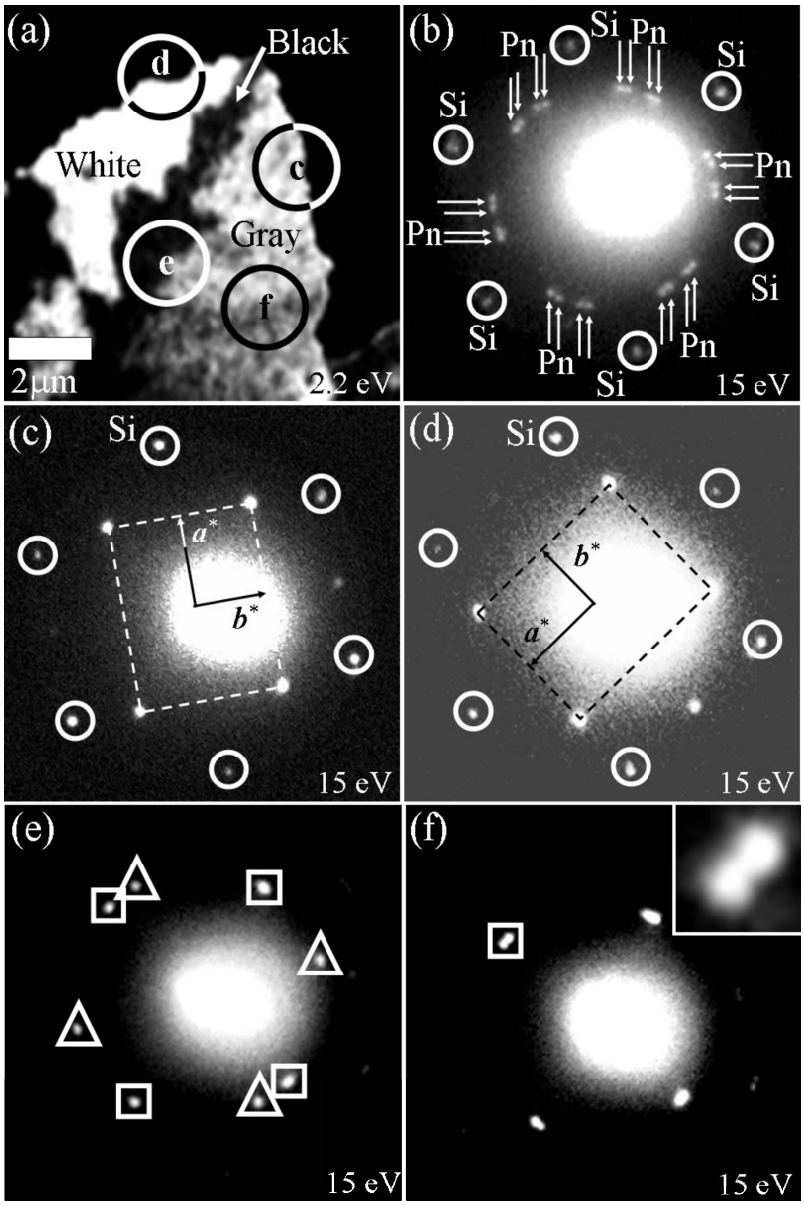

FIG. 1. A polycrystalline domain structure inside a single-monolayer-high Pn dendrite. (a) LEEM image taken in tilted bright-field mode. (b) LEED pattern of Pn dendrite (arrows) and H-Si(111) surface (circles), taken with a selected area of 20 μm diameter, which covers all domains inside dendrite as well as noncovered H-Si(111) surface shown in (a). (c)–(f) μ-LEED patterns taken from areas indicated as open circles c–f in (a). These μ-LEED patterns were taken with a selected area of 2 μm diameter. Dotted rectangles in (c) and (d) correspond to unit cells of Pn thin-film crystals. Open squares and triangles in (e) show diffraction spots observed in area c and those found only in area e, respectively. The (f) inset shows a magnified image of diffraction spots with a 4.6° relative rotation indicated as an open square.

domly adsorbed and wetting layers were formed prior to the subsequent nucleation and growth of thin-film crystals.[9]

In our previous work,[15] we reported that, on a H-Si(111) surface, Pn molecules grow in a standing-up orientation, with the Pn(001) plane parallel to the substrate surface.[15,16] Hence, the four diffraction spots of a Pn single-crystalline area [Figs. 1(c) and 1(d)] correspond to the periodicity in the diagonal directions of a Pn 2D unit cell ($\langle 11 \rangle$ and $\langle 1\bar{1} \rangle$) in the Pn(001) plane—the LEED patterns did not show the (10), (01), $(\bar{1}0)$, and $(0\bar{1})$ spots. The 2D lattice parameters of the single-monolayer-high type-I Pn dendrite on H-Si(111), obtained from the analysis of the LEED patterns, are $|a|=6.02\pm0.01$ Å, $|b|=7.62\pm0.02$ Å, and $\gamma=90.0\pm0.4°$ (Table I). These 2D lattice parameters and their errors were determined from the statistical analysis of 15 μ-LEED patterns after the image distortion was carefully corrected. The most plausible reason for the extinction of the (10), (01), $(\bar{1}0)$, and $(0\bar{1})$ spots is the distortion of the structure of the Pn thin-film crystals from the triclinic bulk structure in such a way that the two molecules within a Pn unit cell become almost equivalent. The 2D lattice parameters obtained in this study are very close to those of the thin-film phase on a SiO_2 surface,[8] but are slightly different from those of the same phase on NaCl(001) (Ref. 17) and Bi(001) (Ref. 18) substrates (particularly γ). Another diffraction study of Pn thin-film crystals on H-Si(111) using a LEED-analog projection technique has been reported recently;[16] however, the structure of the 2D unit cell was different from that of ours.

Figure 2(a) shows the sketch of molecular packing in the Pn dendrite shown in Fig. 1. Rectangular lines represent the unit cell of the Pn layer, and solid lines indicate the directions of Pn molecular planes. On the H-Si(111) surface, Pn molecules are in the standing-up orientation, and Pn molecular planes are slightly tilted to two specific directions. The long (b) axis of the Pn(001) 2D unit cell is rotated $\pm2.3\pm0.3°$ relative to $\langle 1\bar{1}0 \rangle$ directions of the H-Si(111) surface. The relationships among the six equivalent epitaxial orientations

TABLE I. Lattice parameters of (001) planes of pentacene crystals.

	$\|a\|$ (Å)	$\|b\|$ (Å)	γ (deg)
Monolayer on H-Si(111) (type I)[a]	6.02±0.01	7.62±0.02	90.0±0.4
Monolayer on H-Si(111) (type II)	5.98±0.01	7.56±0.01	90.3±0.1
Monolayer on amorphous SiO_2[b]	5.916	7.588	89.95
Thin films on NaCl(100) at high deposition rate[c]	6.1±0.1	7.6±0.1	89.5±0.9
Thin films on NaCl(100) at low deposition rate[c]	6.2±0.1	7.7±0.1	84.8±0.8
Thin films on Bi(001)/Si(111)-7×7[d]	6.1±0.2	7.89	86.0±0.5
Bulk crystal structure[e]	6.266±0.001	7.775±0.001	84.684±0.004

[a]Reference 11.
[b]Reference 8.
[c]Reference 17.
[d]Reference 18.
[e]Reference 7.

found in this study are shown schematically in Fig. 2(b). The directions of the 2D unit cells are almost the same as in those labeled 1 and 4, 2 and 5, and 3 and 6, with an angle of 4.6±0.3° between the *b* axes of the 2D unit cells. These three sets of 2D unit cells with 4.6° relative rotations are depicted at the same contrast level in Fig. 1(a).

The morphology of the Pn dendrite and the domain structure depicted at the three relatively different contrast levels are shown schematically in Fig. 3. The figure also shows a summary of the molecular orientations corresponding to the Pn 2D unit cells having specific epitaxial orientations outlined in Fig. 2(b). We found that the growth directions of the dendritic branches (bold arrows in Fig. 3), which are almost parallel to the directions of the *b* axes of the 2D unit cells in the center domains (broken arrows in Fig. 3), coincide with the $\langle 1\bar{1}0\rangle$ directions for the type-I dendrites. As reported in our previous study,[11] the Pn dendrite has six main branches, each of which is composed of three domains, reflecting the substrate's crystallographic symmetry. In this study, we found that, inside the type-I Pn dendrites, the sets of domains labeled 1, 2, and 3, and 4, 5, and 6 have relative angles of ±120°, and the sets of domains labeled 1 and 4, 2 and 5, and 3 and 6 each possess a relative angle of 4.6°.

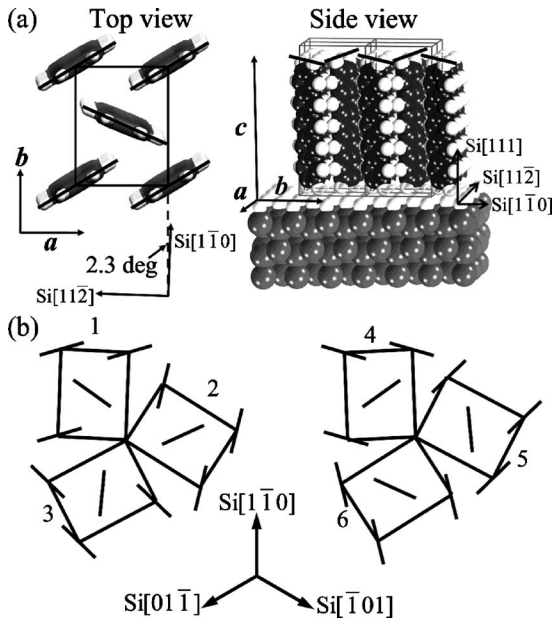

FIG. 2. (a) Molecular packing of Pn in the 2D unit cell of the single-monolayer-high Pn dendrite of type I and (b) six equivalent epitaxial orientations of Pn 2D unit cells. The rectangular lines indicate the unit cell of the Pn layer, and the solid lines indicate the directions of Pn molecular planes. The long (*b*) axes of the Pn 2D unit cells are rotated ±2.3±0.3° relative to $<1\bar{1}0>$ directions of the substrate surface. The unit cells 1 and 4, 2 and 5, and 3 and 6, respectively, make an angle of 4.6±0.3°, and show the same contrast level in our LEEM images because the directions of the Pn 2D unit cells are almost the same.

One of the specific characteristics of the polycrystalline domain structure shown in Fig. 3 is the boundary between adjacent domains. Figure 4(a) shows a scanning tunneling microscopy (STM) image of a domain boundary observed inside a single-monolayer-high Pn dendrite. Since the lattice lines observed in the upper and lower halves of the image show a relative rotation of approximately 120°, the boundary shown in Fig. 4(a) corresponds to that between the domains depicted at different contrast levels in Figs. 1(a) and 3. Fig. 4(b) shows a molecular-resolution STM image of a different type of boundary (from the upper-left direction to lower-right direction of the image). Because protrusions corresponding to individual Pn molecules on both sides of the boundary are fitted into the same lattice, the boundary shown in Fig. 4(b) separates Pn domains in which the tilt directions of Pn molecules are opposite (the direction of the out-of-plane *c* axis is reversed). Because the separation between the molecules along the boundary looks larger than those between the molecules in each single-crystalline area, Pn molecules are likely tilted in the directions shown schematically in Fig. 4(b). Because all the domains composed of six equivalent epitaxial relations are oriented in a definite pattern (Fig. 3), there is no boundary with a random orientation inside the Pn dendrite. In the case of inorganic semiconductor crystals, grain boundaries that have specific crystallographic orientations and a number of lattice points shared by adjacent grains are electrically inactive,[19,20] whereas grain boundaries with random

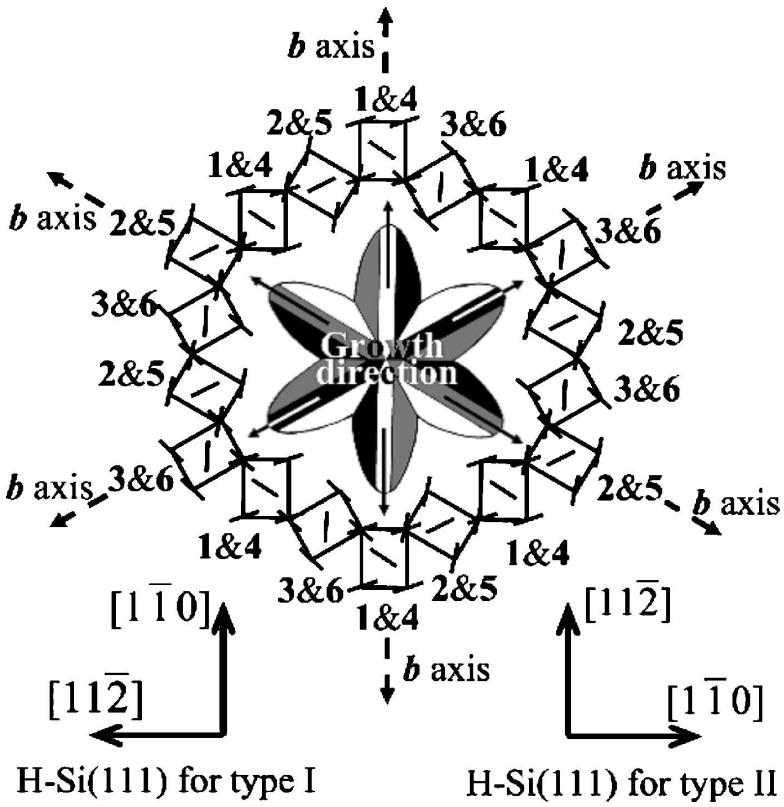

FIG. 3. Schematic illustration of the morphology of Pn dendrite of type I and domain structure depicted at three relatively different contrast levels. The orientations of the 2D unit cells inside the Pn dendrite are also shown. The bold solid arrows correspond to the growth directions of the dendritic branches, and the bold broken arrows show the directions of the *b* axes of the 2D unit cells in the central domains of the dendritic branches. Numbers next to the unit cells correspond to those in Fig. 2(b). For simplicity, the sets of 2D unit cells having small relative rotations (1 and 4, 2 and 5, and 3 and 6) are represented as the same unit cells. Crystallographic directions of H-Si(111) for a type-II Pn dendrite are discussed in Sec. III B.

orientations work as active recombination centers of carriers. If such a relationship between characteristics of boundaries and their electrical properties is also applicable in the case of organic semiconductor thin-film crystals, a polycrystalline domain structure with boundaries of specific orientations would have a weaker adverse effect on electric properties; hence, it would be beneficial to inhibit the generation of random grain boundaries. The electric properties of the polycrystalline domain structure of the Pn dendrite have to be elucidated in the near future.

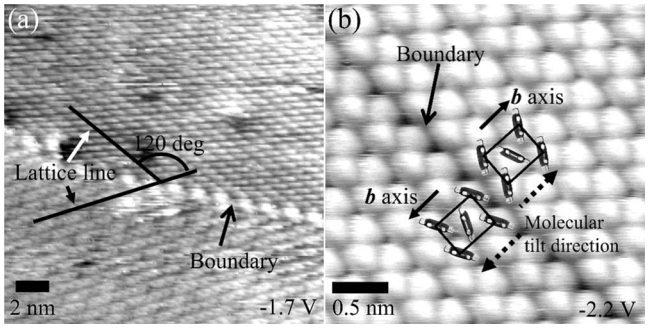

FIG. 4. STM images of boundaries observed inside single-monolayer-high Pn dendrite. (a) Boundary between two rotational Pn domains within single dendrite, equivalent to those depicted at different contrast levels in Figs. 1(a) and 3. (b) Boundary separating Pn domains in which tilt directions of Pn molecules are opposite (the direction of out-of-plane *c* axis is reversed), as shown schematically.

B. Another set of epitaxial relation and lattice coherencies of Pn dendrites

In addition to the epitaxial relation between the thin film and H-Si(111) (type I) shown in Fig. 2, we also found another set of epitaxial relations (type II). Type-II Pn thin-film crystals also grow as dendrites and show a similar domain structure depicted at the three relatively different contrast levels [Fig. 5(a)] in LEEM, as in the case of the type-I dendrites. A LEED pattern taken for a selected area of 20 μm diameter is shown in Fig. 5(b). Systematic LEED analyses revealed that single-monolayer-high Pn dendrites of type II also showed 24 diffraction spots [some of the spots are very faint in Fig. 5(b)]. However, the diffraction spots of the type-II dendrites are rotated approximately 90° in relation to those of the type-I dendrites [Fig. 1(b)]. The μ-LEED patterns shown in Figs. 5(c) and 5(d) [taken from respective selected areas, c and d in Fig. 5(a), of 2 μm diameter] show that the domain depicted at one contrast level in the tilted bright-field LEEM mode is a mixture of two orientations rotated by 7.2° with respect to each other, similar to that in the case of the type-I domain. The 2D lattice parameters of the type-II Pn dendrite, analyzed from the LEED patterns, are $|a|=5.98\pm0.01$ Å, $|b|=7.56\pm0.01$ Å, and $\gamma=90.3\pm0.1°$ (type II in Table I). These 2D lattice parameters are similar to those of type I, although the relation between the Pn layer and H-Si(111) is different.

Figure 5(e) shows the molecular packing of the type-II Pn dendrite. The long (*b*) axis of the type-II 2D unit cell is rotated $\pm3.6\pm0.4°$ relative to the $\langle 11\bar{2}\rangle$ directions of the H-Si(111) surface. We found that the type-II Pn 2D unit cells

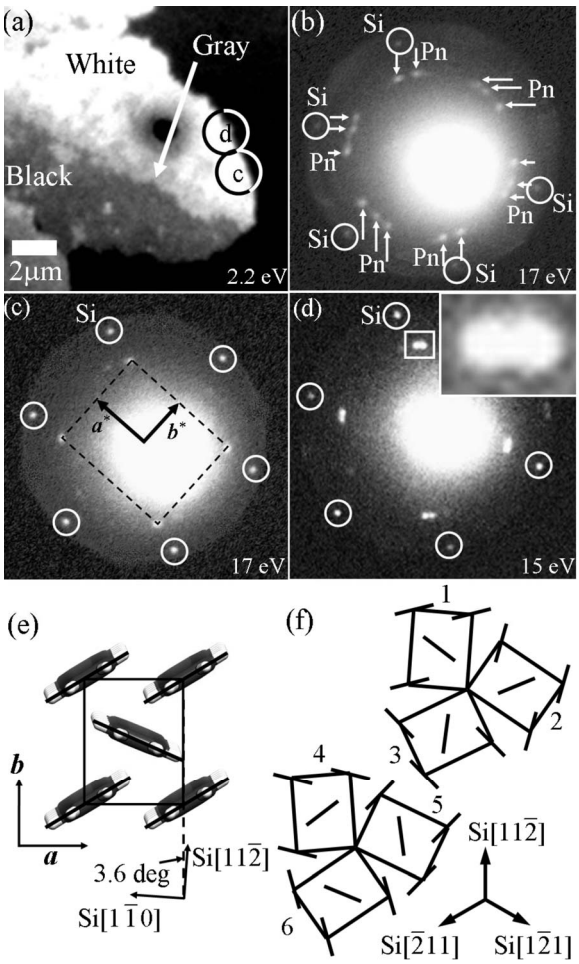

FIG. 5. Polycrystalline domain structure, diffraction patterns, and epitaxial orientations of single-monolayer-high Pn dendrite of type II. (a) LEEM image taken in tilted bright-field mode. (b) LEED pattern of Pn dendrite (arrows) and H-Si(111) surface (circles), taken with a selected area of 20 μm diameter. (c) and (d) μ-LEED patterns taken from areas indicated by open circles c and d in (a), respectively, with a selected area of 2 μm diameter. (e) Molecular packing of Pn in 2D unit cell. The rectangular lines indicate the unit cell of the Pn layer, and the solid lines present the directions of Pn molecular planes. The long (b) axes of the Pn 2D unit cells are rotated $\pm 3.6 \pm 0.4°$ relative to $\langle 11\bar{2} \rangle$ directions of the substrate surface. (f) Six equivalent epitaxial orientations of Pn 2D unit cells. The unit cells 1 and 4, 2 and 5, and 3 and 6, respectively, each make an angle of $7.2 \pm 0.4°$, and show the same contrast level in the tilted bright-field LEEM mode because the Pn 2D unit cells are in almost the same directions.

also have six equivalent epitaxial orientations, as shown schematically in Fig. 5(f). The 2D unit cells of 1 and 4, 2 and 5, and 3 and 6 are rotated 7.2° with respect to each other, and the domains composed of these sets of 2D unit cells show the same contrast level in the tilted bright-field LEEM mode. The high similarity between the structures of the 2D unit cells of types I and II indicates that the interaction between Pn molecules mainly governs the crystal structure of the Pn dendrites on the H-Si(111) surface, although the difference in lattice parameters between the thin films and bulk crystals also suggests that the contribution of H-Si(111) cannot be neglected.

As summarized schematically in Fig. 3, systematic *in situ* LEEM showed that the morphology and domain structure of the type-II Pn dendrite are similar to those of the type-I dendrite, except for the relations between the thin film and H-Si(111). The growth directions of the dendritic branches (bold arrows in Fig. 3) coincide with the $\langle 11\bar{2} \rangle$ directions for the type-II dendrites.

It has to be emphasized that each Pn dendrite is composed of the domain structure of only type I or II, and that there is no dendrite in which the domains of types I and II coexist. This indicates that the boundary between rotational Pn domains of the same type (I or II) is energetically more favorable than that between the domains of different types: once a Pn domain of type I or II nucleates on H-Si(111), only heterogeneous nucleation of the domains of the same type is subsequently allowed to occur on the edge of the domain that developed previously. Thus, the coalescence of the dendrites of the two types should form a new type of domain boundary that is not observed inside the isolated dendrite.

The lattice coherencies of the Pn dendrites of types I and II and H-Si(111) are shown schematically in Fig. 6. We found that the Pn 2D unit cells of both types have the so-called point-on-line coincidences with H-Si(111).[21,22] The black dots in the figure indicate the points at which the lattice points of the Pn 2D unit cells lie on the lattice lines of H-Si(111). For both types, the point-on-line coincidences are much stronger in the direction parallel to the b axes than in the direction parallel to the a axes. The point-on-line coincidence is found for every six cells in the direction parallel to the a axis of the type-I dendrites, whereas it is found for every eight cells in the same direction in the type-II dendrites.

In addition to the point-on-line coincidences, we found supercell structures of the Pn dendrites. Figures 7(a) and 7(b) show μ-LEED patterns taken from single-crystalline areas of the Pn dendrites of types I and II, respectively. For each type, two diffraction spots from supercell structures are observed in the vicinity of the (00) diffraction spot [insets of Figs. 7(a) and 7(b)]. These results indicate that each type has a long-range order in one direction. The type-I dendrite has a periodicity of 36.0 ± 0.8 Å in the direction rotated $0.2 \pm 0.6°$ relative to its a axis, and the type-II dendrite has a periodicity of 16 ± 1 Å in the direction rotated $1.5 \pm 0.6°$ relative to its a axis.

The supercell structure of the type-I dendrite corresponds to the point-on-line coincidence for every six cells in the a-axis direction [Fig. 6(a)] within experimental error. However, the apparent supercell structure of the type-II dendrite based on the assumption that the supercell-related spots in the LEED pattern in Fig. 7(b) are of the first order does not match the adsorption structure deduced from the lattice coherencies. This problem can be overcome if we assume that the direction of the periodicity of the supercell structure matches the a axis and that the supercell diffraction spots observed in Fig. 7(b) are of the third order. These assumptions produce a real space periodicity, 48 ± 1 Å, that is three times larger and matches the point-on-line periodicity

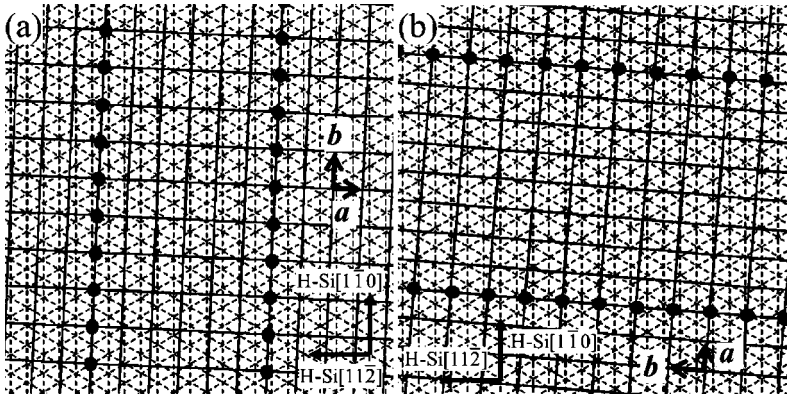

FIG. 6. Schematic illustrations of point-on-line coincidences between Pn dendrites of types (a) I and (b) II and H-Si(111) surface. Solid lines correspond to the lattice lines of the Pn layer, and broken lines correspond to the lattice lines of H-Si(111). Black dots indicate the points at which the lattice points of the Pn 2D unit cells match the lattice lines of H-Si(111).

(47.84±0.01 Å) in the *a*-axis direction. At present, a clear explanation for the extinction of the first and second order supercell diffraction spots is not possible due to the lack of a vital model for the electron scattering mechanisms at the very low energy employed in the experiment. Nevertheless, the existence of supercell structures indicates that slight deformations with long-range periodicities along the *a* axis significantly contribute to the energetic stabilization of Pn dendrites on H-Si(111), in addition to the close point-on-line coincidence for every cell along the *b* axis.

To understand the lattice coherencies and supercell structure of Pn dendrites of types I and II and H-Si(111) quantitatively, the calculation of the interface energy between a Pn dendrite and H-Si(111) is indispensable. However, because the supercell unit is so huge, such calculation is not viable at present. Hence, we evaluated the relation between the density of the point-on-line coincidence and the orientation of the Pn dendrites, as shown in Fig. 8. The vertical axis presents the density of points at which the lattice points of the Pn 2D unit cells lie on the lattice lines of H-Si(111), and the horizontal axis shows the angle between the direction of the *b* axis of the Pn 2D unit cell and the $\langle 1\bar{1}0\rangle$ directions of H-Si(111). We found that three coincidences, labeled I, II, and III, at angles of 2.3°, 26.4°, and 3.8°, respectively, have significantly higher commensurabilities than the others. Coincidences I and II indicate the Pn dendrites of types I and II (for the type-II dendrite, the angle of 26.4° corresponds to an angle of 3.6° relative to the $\langle 11\bar{2}\rangle$ direction). The appearances of the dendrites with the highest two commensurabilities are clearly observed in our experiments. The results presented in Fig. 8 suggest that the type-I dendrite is energetically more stable than the type-II dendrite. Among the 123 Pn dendrites we investigated, the probabilities of finding dendrites of types I and II were 67% and 33%, respectively. The higher commensurability of the type-I dendrites and H-Si(111) results in a higher probability of finding type-I dendrites.

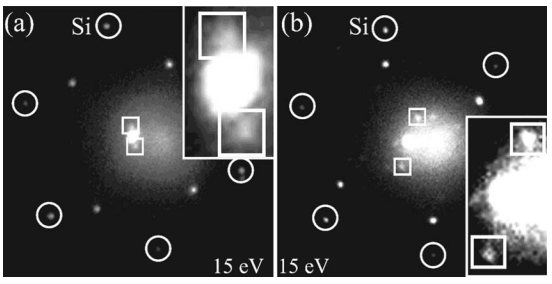

FIG. 7. Supercell structures observed in μ-LEED patterns of Pn dendrites of types (a) I and (b) II. Diffraction spots from the supercell structures of single-crystalline areas are indicated as open squares, and H-Si(111)-related spots are marked by open circles. Insets show magnified images of supercell-related spots. These μ-LEED patterns were taken with a selected area of 2 μm diameter. The contrast level of the supercell-related spots in the vicinity of the (00) spot was enhanced by image processing, although H-Si(111)-related spots became faint.

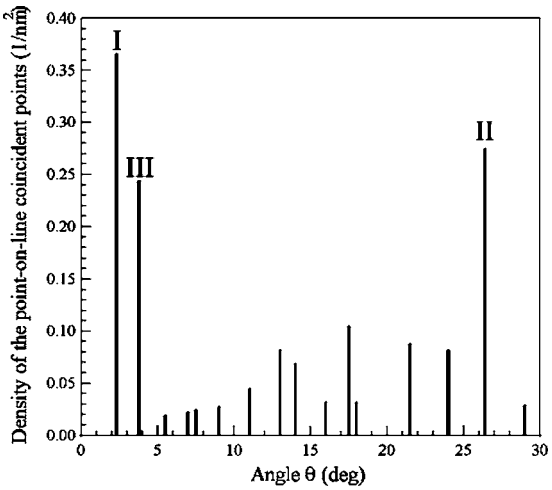

FIG. 8. Point-on-line coincidence versus in-plane orientation of Pn 2D lattice. The vertical axis shows the density of the points at which the lattice points of Pn 2D unit cells lie on lattice lines of H-Si(111), and the horizontal axis shows the angle between the direction of the *b* axis of a Pn 2D unit cell and the $\langle 1\bar{1}0\rangle$ directions of H-Si(111). The angle of 30° indicates the $\langle 11\bar{2}\rangle$ directions of H-Si(111). Because of the crystallographic symmetry, only the angular range of 0–30° is shown in this figure. Coincidence I corresponds to type-I dendrites (2.3°), and coincidence II corresponds to type-II dendrites [26.4°: 3.6° relative to the $\langle 11\bar{2}\rangle$ directions of H-Si(111)]. The coincidence at 3.8° (III) shows the possible formation of another set of epitaxial relations between Pn thin films and H-Si(111).

In contrast to those with coincidences I and II, no actual Pn islands with coincidence III (3.8°) were found in our experiment, although it also has a considerably high commensurability (the angular difference between coincidences I and III can be detected by LEED analysis). We expect that even when the Pn islands with coincidence III are nucleated, they would be transformed into type-I dendrites because of the small angular difference (1.5°) between coincidences I and III. No islands with other much smaller commensurabilities were observed in our experiment.

To study the effects of the commensurability of types I and II on the dendrite growth of Pn, we grew Pn dendrites on H-Si(111) at deposition rates of 0.05 and 0.5 ML/min, and observed the morphology of Pn dendrites in the tilted bright-field LEEM imaging mode. The fractal dimensions D_f measured by a box counting method[23] are 1.76±0.03 (low deposition rate) and 1.70±0.03 (high deposition rate) for the type-I dendrites, and 1.79±0.05 (low deposition rate) and 1.71±0.02 (high deposition rate) for the type-II dendrites. Although the basic structures of all the dendrites were the same, note that the Pn dendrites grown at the higher deposition rate are more dendritic in shape and, hence, have smaller fractal dimensions. This result can be explained by a larger Berg effect[24] promoted by a higher deposition rate. The D_f values of types I and II at the higher deposition rate coincide well with the theoretical value of 1.71 for the case of diffusion-limited aggregation.[25] In contrast, the morphological changes between types I and II were the same within experimental error despite the significant difference observed between the nucleations of types I and II (67% and 33%) caused by the difference in the commensurability with H-Si(111). These results suggest that, under our experimental conditions, the difference in the commensurability with H-Si(111) does not markedly affect the growth kinetics at the edges of the dendrites and, hence, the factors related to the crystal structure of Pn thin films, such as the interaction between Pn molecules and steric hindrance during the incorporation, predominantly determine the growth kinetics of Pn dendrites.

C. Estimation of interface energy between Pn dendrites and H-Si(111)

Under all the experimental conditions adopted in this study, single-monolayer-high Pn dendrites were formed, and no crystal with a three-dimensional (3D) island shape was observed. Therefore, from this observation, we attempted to roughly estimate the interface energy between the Pn dendrite and H-Si(111). For simplicity, we calculated the free energy of a cylindrical Pn island of radius r and height h grown on H-Si(111). The free energy ΔG of the island can be expressed as[26]

$$\Delta G = -\frac{V}{\Omega}\Delta\mu + 2\pi rh\chi + \pi r^2(\sigma + \sigma_i - \sigma_s), \tag{1}$$

where V is the volume of the island, Ω the volume of one Pn molecule, $\Delta\mu$ the driving force for crystallization, χ the surface energy of the lateral side of the island, σ the surface energy of the top face of the island, σ_i the excess free energy of the interface between the island and the substrate, and σ_s the surface energy of the substrate. The excess free energy of the interface can be defined as[27]

$$\sigma_i = \sigma_s + \sigma - \phi_{Pn\text{-}sub}, \tag{2}$$

where $\phi_{Pn\text{-}sub}$ is the binding energy at the Pn–H-Si(111) heteroepitaxial interface for a unit area. Substituting Eq. (2) into Eq. (1) and eliminating r and h using an aspect ratio of the island $R=h/r$, one obtains

$$\Delta G = -\frac{V}{\Omega}\Delta\mu + \pi^{1/3}V^{2/3}[2\chi R^{1/3} + (2\sigma - \phi_{Pn\text{-}sub})R^{-2/3}]. \tag{3}$$

In Eq. (3), to evaluate $\Delta\mu$, we measured the flux $J(T_{cru})$ of the Pn molecular beam as a function of the crucible temperature T_{cru} using a quartz crystal microbalance and evaluated the flux $J(T_{sub})$ of Pn at the substrate temperature T_{sub}. Then from $T_{cru}=145$ °C and $T_{sub}=30$ °C adopted in the LEEM experiments and the relation $\Delta\mu=k_BT_{sub}\times\ln\{J(T_{cru})/J(T_{sub})\}$ (k_B the Boltzmann constant),[28] we obtained $\Delta\mu\approx0.32$ eV/molecule. To evaluate χ and σ, we used the surface energies of the low-index faces of Pn bulk crystals, obtained by Northrup *et al.*, with first-principles pseudopotential density-functional calculations.[29] They calculated the surface energies of (001), (100), (010), (110), and $(\bar{1}10)$ faces to be 3.1×10^{17}, 6.4×10^{17}, 4.8×10^{17}, 4.8×10^{17}, and 4.7×10^{17} eV/m^2, respectively.[29,30] From these calculation results, we adopted $\sigma\approx3.1\times10^{17}$ eV/m^2. As shown schematically in Fig. 9(a), the largest lateral side of the Pn island is close to the (120) and $(\bar{1}20)$ faces. Although the surface energies of these two faces were not calculated by Northrup *et al.*, we adopted the average of the (110) and $(\bar{1}10)$ faces: $\chi\approx4.8\times10^{17}$ eV/m^2.

Using the above values, we attempted to estimate the minimum $\phi_{Pn\text{-}sub}$. Figures 9(b) and 9(c) show changes in ΔG as a function of the aspect ratio R at various $\phi_{Pn\text{-}sub}$ values [numbers of Pn molecules included in a Pn island V/Ω: (b) 10^5 and (c) 10^{10}]. Note that under a high R region, the ΔG of the island increases with increasing R irrespective of V/Ω and $\phi_{Pn\text{-}sub}$. This result demonstrates that the higher R (corresponding to 3D island growth) is energetically less favorable because of the larger area of the unfavorable lateral side of the island. The contribution of the unfavorable lateral side is stronger for a smaller island [Fig. 9(b)] because of the larger specific surface area of the island. In contrast, under a low R region, changes in ΔG with decreasing R strongly depend on $\phi_{Pn\text{-}sub}$. This dependence is stronger for a larger island [Fig. 9(c)] because of the larger interface area of the island. The arrows in Figs. 9(b) and 9(c) show R corresponding to single-monolayer-high islands. In Fig. 9(b), $\phi_{Pn\text{-}sub}=6.15\times10^{17}$ eV/m^2 is sufficient so that a single-monolayer-high island with $R=9.39\times10^{-3}$ becomes most energetically stable; we define such $\phi_{Pn\text{-}sub}$ as $\phi_{Pn\text{-}sub}^{single}$. Figure 9(c) shows that a larger island needs a larger $\phi_{Pn\text{-}sub}^{single}$ (6.20×10^{17} eV/m^2) because of the increase in the interface area. The relation between $\phi_{Pn\text{-}sub}^{single}$ and V/Ω is summarized in Fig. 9(d). With increasing V/Ω, $\phi_{Pn\text{-}sub}^{single}$ increases significantly,

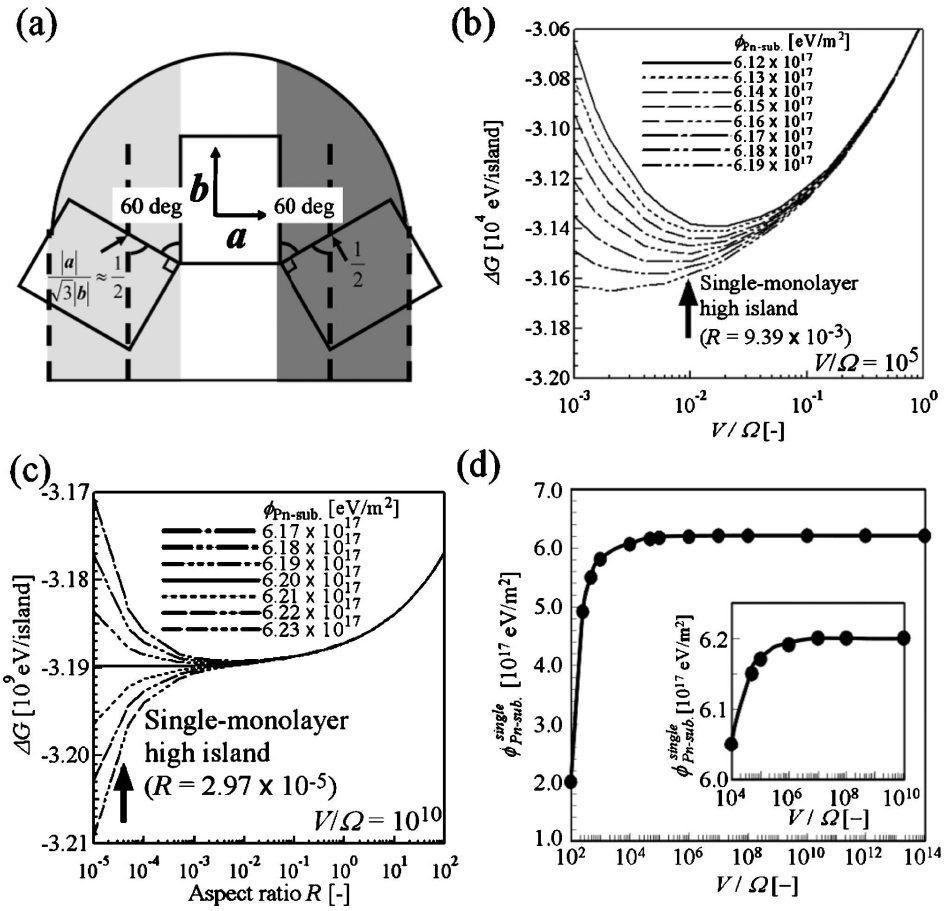

FIG. 9. Estimation of interface energy between Pn dendrite and H-Si(111). (a) Schematic illustration of polycrystalline domain structure of dendrite branch and orientations of 2D unit cells inside domains. (b) and (c) Changes in free energy ΔG of Pn island as a function of an aspect ratio R at various $\phi_{Pn\text{-}sub}$ values. Numbers of Pn molecules included in an island V/Ω: (b) 10^5 and (c) 10^{10}. Arrows show the aspect ratios of single-monolayer-high islands. The single-monolayer-high island of $V/\Omega=10^{10}$ corresponds to an island with a diameter of 54 μm, which is very close to the average diameter of 50 μm observed in this study. (d) Changes in $\phi_{Pn\text{-}sub}^{single}$, which is the $\phi_{Pn\text{-}sub}$ necessary to make a single-monolayer-high island most energetically stable, as a function of V/Ω. The inset shows $\phi_{Pn\text{-}sub}^{single}$ in the range of $V/\Omega=10^4-10^{10}$.

and then reaches a constant value of 6.20×10^{17} eV/m^2 under $V/\Omega\geqslant10^7$, which is sufficiently smaller than that ($V/\Omega=10^{10}$) of the island observed experimentally in this study. Therefore, we conclude that $\phi_{Pn\text{-}sub}\geqslant6.20\times10^{17}$ eV/m^2 is necessary to reproduce the single-monolayer-high Pn island observed in the experiments. In addition, we also carried out similar calculations by changing χ from 3.1×10^{17} to 6.4×10^{17} eV/m^2 (data not shown), and found that the minimum $\phi_{Pn\text{-}sub}$ to reproduce the single-monolayer-high Pn island is 6.20×10^{17} eV/m^2 irrespective of χ.

As reported previously (Fig. 2 in Ref. 15), the number density of Pn islands formed on top of the first Pn layer is higher than that of the first Pn layer formed on H-Si(111). This suggests that the binding energy between the first and second Pn layers ($\phi_{Pn\text{-}Pn}=2\sigma\approx6.2\times10^{17}$ eV/m^2) is stronger than that between the first Pn layer and H-Si(111) ($\phi_{Pn\text{-}sub}$). However, the minimum $\phi_{Pn\text{-}sub}$ estimated from Fig. 9 is the same as $\phi_{Pn\text{-}Pn}$. This small contradiction would be due not only to the uncertainties of the values of σ and χ, but also to our estimation method, in which we calculated only ΔG and, hence, neglected the contribution of kinetic processes (nonequilibrium phenomena) during crystallization, although the dendritic shape of the Pn layer indicates that the real growth conditions were far from equilibrium. In addition, we also point out the limit of our model where an island is considered as a continuum. When R becomes small enough, discreteness of molecular layers has to be taken into account. However, we believe that our model is worthy to provide a rough estimation of an interface energy of a heteroepitaxially grown thin film from its aspect ratio.

IV. CONCLUSIONS

We observed single-monolayer-high Pn dendrites grown on H-Si(111) by LEEM and μ-LEED analyses. We found two sets of epitaxial relations (types I and II) between the Pn dendrites and H-Si(111). The Pn dendrites of both types have six equivalent epitaxial orientations and similar polycrystalline domain structures, in which three sets of 2D unit cells that are rotated ±120° relative to each other exist. Each dendrite has six branches, each composed of three domains depicted at different contrast levels in the tilted bright-field LEEM mode, where the domain depicted at one contrast level is a mixture of two orientations with a small relative rotation (type I: 4.6° and type II: 7.2°). The boundaries inside the dendrite were successfully observed by STM. We also determined the 2D lattice parameters of both dendrite types, whose values are almost the same; the 2D unit cells of both types are rotated approximately 90° relative to each other. These results indicate that the interaction between Pn molecules mainly determines the crystal structure of the dendrites on H-Si(111). Each Pn dendrite is composed of domains exclusively of type I or II.

The so-called point-on-line coincidences are found between the Pn 2D lattices of both types and H-Si(111). The

higher commensurability of the type-I dendrites than that of the type-II dendrites results in a higher probability of finding type-I dendrites. For the Pn dendrites of both types, we also found supercell structures, which contribute to the energetic stabilization of the Pn dendrites on H-Si(111). We estimated the minimum interface energy, between the Pn dendrite and H-Si(111) from the island's free energy, necessary to reproduce the growth of a single-monolayer-high Pn dendrite.

ACKNOWLEDGMENTS

This work was partially supported by Project Research B of the Center for Interdisciplinary Research, Tohoku University. One of the authors (G.S.) thanks the partial support in the form of a Grant-in-Aid (Grant No. 16656004) for Scientific Research from the Ministry of Education, Culture, Sports, Science, and Technology, Japan.

*Author to whom correspondence should be addressed; sazaki@cir.tohoku.ac.jp

[1] C. D. Dimitrakopoulos, S. Purushothaman, J. Kymissis, A. Callegari, and J. M. Shaw, Science **283**, 822 (1999).
[2] A. R. Brown, A. Pomp, C. M. Hart, and D. M. de Leeuw, Science **270**, 972 (1995).
[3] S. F. Nelson, Y. Y. Lin, D. J. Gundlach, and T. N. Jackson, Appl. Phys. Lett. **72**, 1854 (1998).
[4] C. D. Dimitrakopoulos, I. Kymissis, S. Purushothaman, D. A. Neumayer, P. R. Duncombe, and R. B. Laibowitz, Adv. Mater. (Weinheim, Ger.) **11**, 1372 (1999).
[5] R. B. Campbell, J. M. Robertson, and J. Trotter, Acta Crystallogr. **14**, 705 (1961).
[6] R. B. Campbell and J. M. Robertson, Acta Crystallogr. **15**, 289 (1962).
[7] C. C. Mattheus, A. B. Dros, J. Baas, A. Meetsma, J. L. de Boer, and T. T. M. Palstra, Acta Crystallogr., Sect. C: Cryst. Struct. Commun. **57**, 939 (2001).
[8] S. E. Fritz, S. M. Martin, C. D. Frisbie, M. D. Ward, and M. F. Toney, J. Am. Chem. Soc. **126**, 4084 (2004).
[9] F.-J. M. Zu Heringdorf, M. C. Reuter, and R. M. Tromp, Nature (London) **412**, 517 (2001).
[10] R. Ruiz, B. Nickel, N. Koch, L. C. Feldman, R. F. Haglund, A. Kahn, and G. Scoles, Phys. Rev. B **67**, 125406 (2003).
[11] J. T. Sadowski, G. Sazaki, S. Nishikata, A. Al-Mahboob, Y. Fujikawa, K. Nakajima, R. M. Tromp, and T. Sakurai, Phys. Rev. Lett. **98**, 046104 (2007).
[12] E. Bauer, Rep. Prog. Phys. **57**, 895 (1994).
[13] S. Suto, R. Czajka, S. Szuba, A. Shiwa, S. Winiarz, H. Nagashima, H. Kato, T. Yamada, and A. Kasuya, Acta Phys. Pol. A **104**, 289 (2003).
[14] H. Kato, T. Taoka, S. Nishikata, G. Sazaki, T. Yamada, R. Czajka, A. Wawro, K. Nakajima, A. Kasuya, and S. Suto, Jpn. J. Appl. Phys. **46**, 5701 (2007).
[15] S. Nishikata, G. Sazaki, T. Takeuchi, N. Usami, S. Suto, and K. Nakajima, Cryst. Growth Des. **7**, 439 (2007).
[16] T. Shimada, H. Nogawa, T. Hasegawa, R. Okada, H. Ichikawa, K. Ueno, and K. Saiki, Appl. Phys. Lett. **87**, 061917 (2005).
[17] J. S. Wu and J. C. H. Spence, J. Appl. Crystallogr. **37**, 78 (2004).
[18] J. T. Sadowski, T. Nagao, S. Yaginuma, Y. Fujikawa, A. Al-Mahboob, K. Nakajima, T. Sakurai, G. E. Thayer, and R. M. Tromp, Appl. Phys. Lett. **86**, 073109 (2005).
[19] A. Fedotov, B. Evtodyi, L. Fionova, Yu Ilyashuk, E. Katz, and L. Polyak, Phys. Status Solidi A **119**, 523 (1990).
[20] Z. J. Wang, S. Tsurekawa, K. Ikeda, T. Sekiguchi, and T. Watanabe, Interface Sci. **7**, 197 (1999).
[21] A. Hoshino, S. Isoda, H. Kurata, and T. Kobayashi, J. Appl. Phys. **76**, 4113 (1994).
[22] A. Hoshino, S. Isoda, H. Kurata, and T. Kobayashi, J. Cryst. Growth **146**, 636 (1995).
[23] H.-O. Peitgen, H. Jürgens, and D. Saupe, *Chaos and Fractals New Frontiers of Science* (Springer-Verlag, New York, 1992), p. 212.
[24] W. F. Berg, Proc. R. Soc. London, Ser. A **164**, 79 (1938).
[25] Y. Saito, *Statistical Physics of Crystal Growth* (World Scientific, Singapore, 1996), p. 82.
[26] I. V. Markov, *Crystal Growth for Beginners*, 2nd ed. (World Scientific, New Jersey, 2003), p. 99.
[27] I. V. Markov, *Crystal Growth for Beginners*, 2nd ed. (World Scientific, New Jersey, 2003), p. 19.
[28] I. V. Markov, *Crystal Growth for Beginners*, 2nd ed. (World Scientific, New Jersey, 2003), p. 4.
[29] J. E. Northrup, M. L. Tiago, and S. G. Louie, Phys. Rev. B **66**, 121404(R) (2002).
[30] The definition of crystallographic axes in this study is different from that of Northrup *et al.* (Ref. 29).